
This is an electronic reprint of the original article.
This reprint may differ from the original in pagination and typographic detail.

Björkman, Torbjörn; Skakalova, Viera; Kurasch, Simon; Kaiser, Ute; Meyer, Jannik C.; Smet, Jurgén H.; Krasheninnikov, Arkady V.

Vibrational Properties of a Two-Dimensional Silica Kagome Lattice

Published in:
ACS Nano

DOI:
[10.1021/acsnano.6b05577](https://doi.org/10.1021/acsnano.6b05577)

Published: 27/12/2016

Document Version
Publisher's PDF, also known as Version of record

Published under the following license:
CC BY

Please cite the original version:
Björkman, T., Skakalova, V., Kurasch, S., Kaiser, U., Meyer, J. C., Smet, J. H., & Krasheninnikov, A. V. (2016). Vibrational Properties of a Two-Dimensional Silica Kagome Lattice. *ACS Nano*, 10(12), 10929-10935. <https://doi.org/10.1021/acsnano.6b05577>

This material is protected by copyright and other intellectual property rights, and duplication or sale of all or part of any of the repository collections is not permitted, except that material may be duplicated by you for your research use or educational purposes in electronic or print form. You must obtain permission for any other use. Electronic or print copies may not be offered, whether for sale or otherwise to anyone who is not an authorised user.

Vibrational Properties of a Two-Dimensional Silica Kagome Lattice

Torbjörn Björkman,^{*,†,‡,⊥} Viera Skakalova,^{‡,#} Simon Kurasch,[¶] Ute Kaiser,[¶] Jannik C. Meyer,[‡] Jurgen H. Smet,[§] and Arkady V. Krasheninnikov^{¶,⊥}

[†]Physics/Department of Natural Sciences, Åbo Akademi, Turku FI-20500, Finland

[‡]Faculty of Physics, University of Vienna, Boltzmanngasse 5, Wien 1190, Austria

[¶]Electron Microscopy Group of Materials Science, University of Ulm, Ulm 89081, Germany

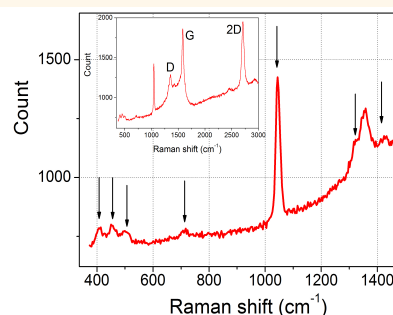
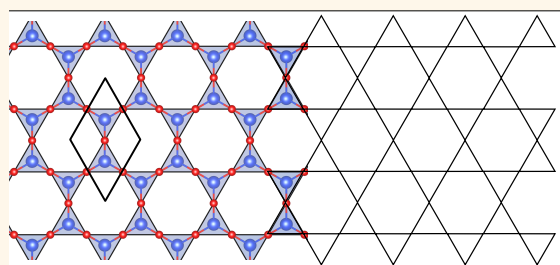
[§]Max Planck Institute for Solid State Research, Stuttgart 70569, Germany

[¶]Institute of Ion Beam Physics and Materials Research, Helmholtz-Zentrum Dresden-Rossendorf, Dresden 01328, Germany

[⊥]Department of Applied Physics, Aalto University School of Science, P.O. Box 11100, Aalto 00076, Finland

[#]STU Center for Nanodiagnostics, Vazovova 5, Bratislava 81243, Slovakia

Supporting Information



ABSTRACT: Kagome lattices are structures possessing fascinating magnetic and vibrational properties, but in spite of a large body of theoretical work, experimental realizations and investigations of their dynamics are scarce. Using a combination of Raman spectroscopy and density functional theory calculations, we study the vibrational properties of two-dimensional silica (2D-SiO₂), which has a kagome lattice structure. We identify the signatures of crystalline and amorphous 2D-SiO₂ structures in Raman spectra and show that, at finite temperatures, the stability of 2D-SiO₂ lattice is strongly influenced by phonon–phonon interaction. Our results not only provide insights into the vibrational properties of 2D-SiO₂ and kagome lattices in general but also suggest a quick nondestructive method to detect 2D-SiO₂.

KEYWORDS: 2D materials, 2D silicon dioxide, kagome, anharmonicity, Raman spectroscopy, density functional theory

The kagome lattice¹ has long been a model system for theoretical studies of various physical properties, primarily magnetism, in systems with particular topology, as it exhibits spin frustration when interactions are antiferromagnetic on a triangular lattice. The mechanical properties of such systems are also of interest.^{2–4} It was theoretically shown that if the kagome lattice consists of rigid triangles that interact only through their direct links (nearest-neighbor interaction), the system becomes isostatic, which means it is on the border of mechanical instability, since compression of the lattice in this case would lead to rotations of the triangles, as shown in Figure 1d, at no cost in energy. Two-dimensional silica (2D-SiO₂) has attracted attention, as it is one of the thinnest insulating materials which can be used in catalysis and for isolating graphene from metal substrates, making vertical heterostructures^{5–9} that can be transferred

between substrates.¹⁰ However, in spite of the substantial progress in its synthesis, little is known about vibrational properties of this 2D system and its Raman spectra. Moreover, it is desirable to have a quick nondestructive technique, such as Raman spectroscopy (RS) to identify this material.

Here we show that the crystalline 2D-SiO₂ structure represents a kagome lattice. Using a combination of Raman spectroscopy and first-principles calculations, we perform an in-depth investigation of the lattice dynamics and find that the stability of 2D-SiO₂ is strongly influenced by phonon–phonon interaction at finite temperatures. We further demonstrate that

Received: August 18, 2016

Accepted: November 9, 2016

Published: November 9, 2016

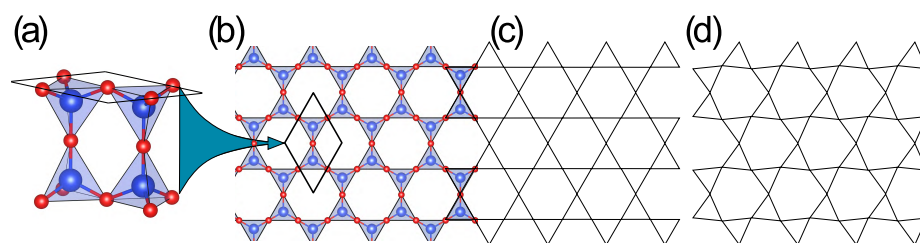


Figure 1. 2D-SiO₂ as a kagome lattice. (a) One unit cell of 2D-SiO₂, in side view, showing the SiO₄ tetrahedra that function as building blocks in nearly all SiO₂ structures. (b) Top view of the structure indicating the unit cell of the hexagonal *P6/mmm* lattice and (c) its interpretation as a linked hexagonal network of equilateral triangles, a kagome lattice. (d) A rotated kagome lattice, which is the ground state of 2D-SiO₂ under compressive strain at zero temperature.¹¹

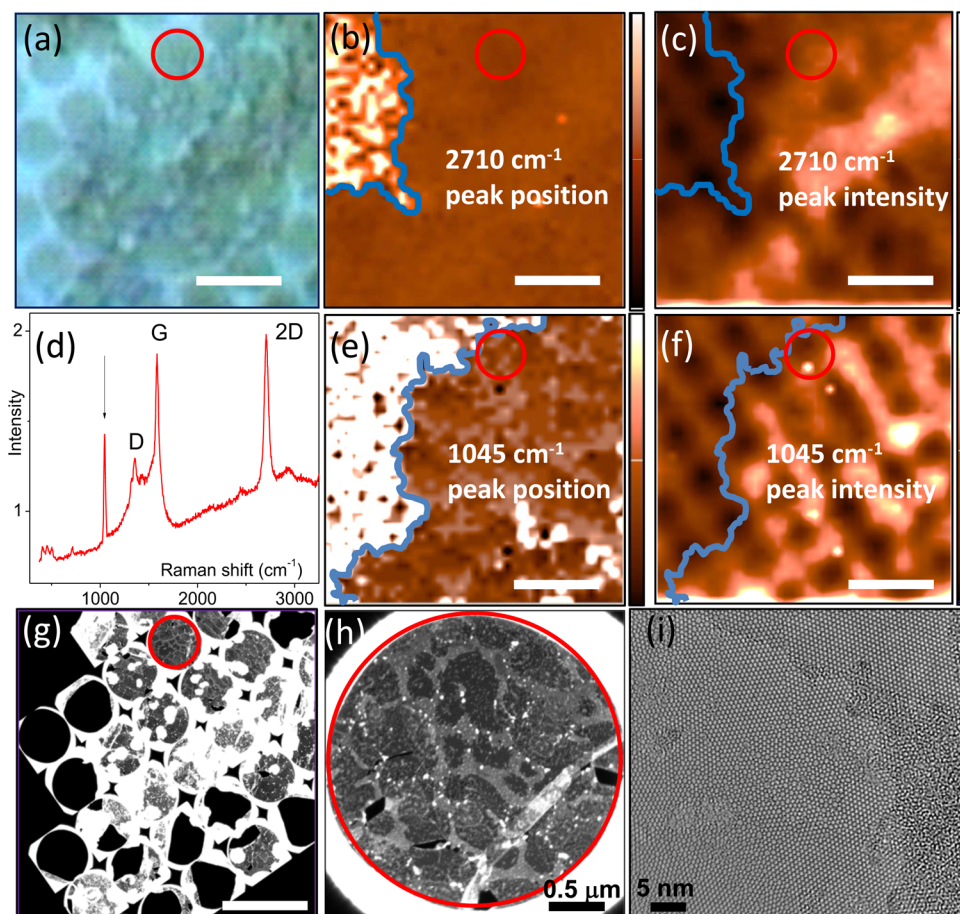


Figure 2. (a) Optical image of a TEM grid covered by graphene and 2D-SiO₂. Maps of Raman peak (b) position and (c) intensity of graphene 2D-band at 2710 cm⁻¹. (d) Raman spectrum measured in the middle of (a). Maps of Raman peak (e) position and (f) intensity at 1045 cm⁻¹. (g) Collection of dark-field TEM images of individual holes in the same area. Scale bars in (a) to (g) correspond to 5 μm. (h) Dark-field TEM image of the hole marked with the red circle in larger magnification. (i) Atomic structure found within the location in (h) identified as 2D-SiO₂. Color rendition bars on the right of the Raman maps refer to values in Z direction: For peak position maps, in (b) the center mark stands for value 2710 cm⁻¹ and in (e) for 1045 cm⁻¹. The extreme dark and bright colors represent ±30 cm⁻¹ deviation from these values. In the intensity map of 2710 cm⁻¹ peak (c), the counts vary from 0 (dark) to 40 × 10³ (bright), and in the intensity map of 1045 cm⁻¹ peak (e), the counts vary from 0 (dark) to 1400 (bright).

there is a characteristic signature of 2D silica in RS, so that this technique, along with infrared spectroscopy,⁵ can be used for a quick identification of the material.

RESULTS AND DISCUSSION

The optical image in Figure 2a shows a section of a TEM grid covered with graphene (details of methods are given in the Supporting Information). The additional layer deposited on top of graphene, well visible in the optical image, is 2D-SiO₂. The

Raman spectrum measured in the middle of the area displayed in Figure 2a is presented in Figure 2d (larger version in Figure S1). It shows the prominent G, D, and 2D peaks, three well-known signatures of graphene. A peak intensity ratio I_G/I_{2D} close to 1 and full width at half-maximum (fwhm) of the 2D peak reaching 50 cm⁻¹ indicate that bi- or trilayer graphene covers the TEM grid in that region. The spectrum baseline mainly results from an amorphous carbon membrane (Quantifoil) covering the TEM gold grid with a typical broad

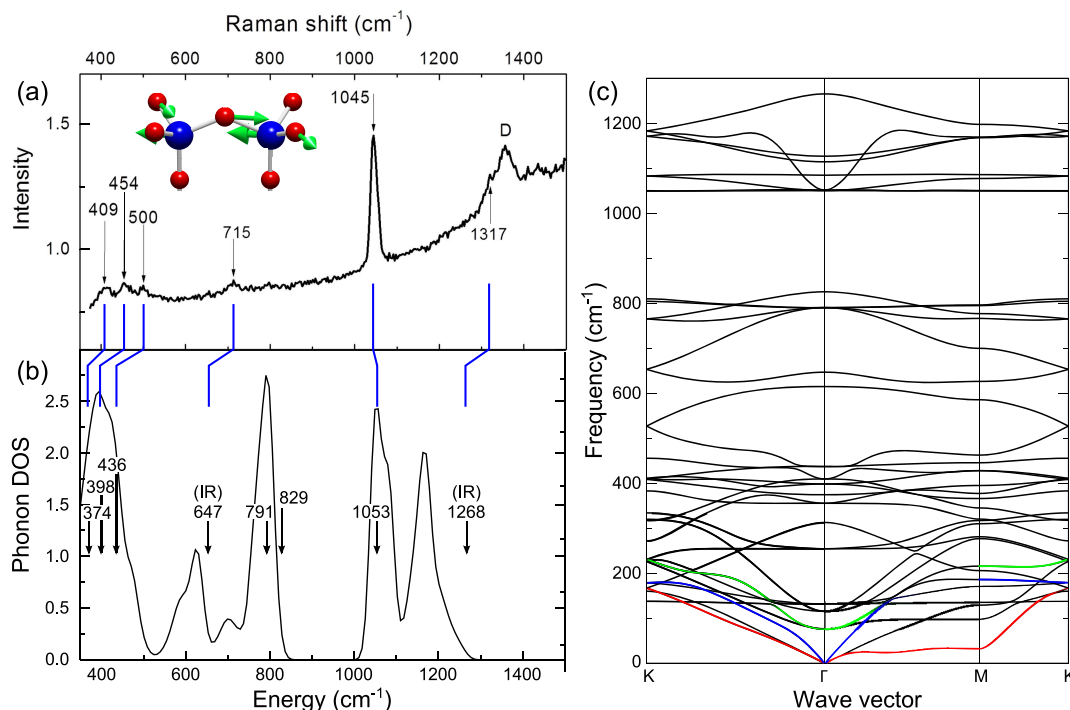


Figure 3. Experimental Raman spectrum (a) and calculated phonon DOS (b) and phonon dispersion graphs (c) for 2D-SiO₂. The positions of optically active modes at the Γ point are marked with arrows in the calculated spectrum, including two IR modes, allowing for identification of experimental modes by correlation to those calculated from DFT (indicated by blue lines between panels (a) and (b)). The inset in (a) shows the antisymmetric bond stretch mode responsible for the prominent peak at 1045 cm⁻¹. The modes colored red, blue, and green in (c) are kagome lattice modes discussed in detail in relation to Figure 4.

background between 1300 and 1600 cm⁻¹. Apart from the graphene features, a distinctive, very narrow (fwhm 20 cm⁻¹) peak at 1045 cm⁻¹ is apparent in the spectrum.

In order to localize the origin of this peak that cannot be assigned to graphene, mapping of Raman spectra in the displayed area was performed. Figure 2b,c shows Raman maps of the peak position and peak intensity of the graphene 2D band at 2710 cm⁻¹. Except for the left upper corner, the brown-colored area shows graphene homogeneously spread over the rest of the square. Raman maps of the peak position and intensity of the feature at 1045 cm⁻¹ are displayed in Figure 2e,f. Here the area where the 1045 cm⁻¹ mode is missing (white, in Figure 2e) is larger than the area where the 2D band of graphene is not present.

In the next step, the same sample area was investigated by HR-TEM. A mosaic composed of dark-field TEM images of the individual holes in the same area of the TEM grid previously studied by Raman mapping is displayed in Figure 2g. For the HR-TEM structural study, we chose a particular position on the grid marked here by a red circle. Imaging the area inside the red circle in Figure 2h in dark-field shows inhomogeneous brighter and darker regions decorated with small white particles. Zooming in even more, the atomic structure obtained in HR-TEM mode and displayed in Figure 2i confirms that the deposited layer on graphene indeed contains 2D-SiO₂, as described in our previous works.¹²

A magnification of the range 400–1500 cm⁻¹ (Figure 3a) reveals that, in addition to the intensive narrow mode at 1045 cm⁻¹, there are also much weaker peaks at 409, 454, 500, and 715 cm⁻¹. Even though there are reports on the Raman active mode at 1045 cm⁻¹ in several bulk systems that contained Si–O–Si bonds,^{13–15} it is not clear how this can be related to the

significantly different 2D structure of 2D-SiO₂. The origin of this mode in bulk systems had long been under dispute, and finally, it was assigned to a Si–O–Si stretching mode, when oxygen bridges silicon atoms with an angle of 180°. This interpretation seems to be possible also in our bilayer silica, since Si–O–Si forms a straight line in the planar structure.

In order to ascertain the origin of the measured Raman modes in 2D-SiO₂, the vibrational properties were investigated by DFT calculations. Figure 3a,b compares the measured Raman spectrum with the phonon density of states (DOS) in the interval containing the vibrational modes seen in the experiments, with arrows marking the optically active modes at the Γ point of the Brillouin zone (Table S1). There is a good agreement for the conspicuous peak at 1045 cm⁻¹. This corresponds to the calculated Raman active E_{1g} mode at 1053 cm⁻¹, an asymmetric bond stretching mode illustrated as an inset in Figure 3a.

With the exception of the bond stretching E_{1g} mode, the calculations appear to consistently underestimate the vibrational frequencies by approximately 8–10%, and a systematic underestimate was also noted by Löffler for calculated IR frequencies.⁵ With this systematic error, the overall agreement is reasonably good, and it allows us to identify and assign symmetry labels for the observed modes as A_{1g} (409 cm⁻¹), E_{1g} (454 cm⁻¹), E_{2g} (500 cm⁻¹), A_{2u} (715 cm⁻¹, IR), E_{1g} (1045 cm⁻¹), and A_{2u} (1317 cm⁻¹, IR). Two Raman active modes at 791 and 829 cm⁻¹ are absent in the experiments, presumably too weak to be visible. The assignment of formally Raman inactive IR modes in the spectrum is somewhat counter-intuitive, but IR modes have been previously reported in Raman spectra due to breaking of inversion symmetry, which may be caused by the sample geometry of thin films,¹⁶ a 2D

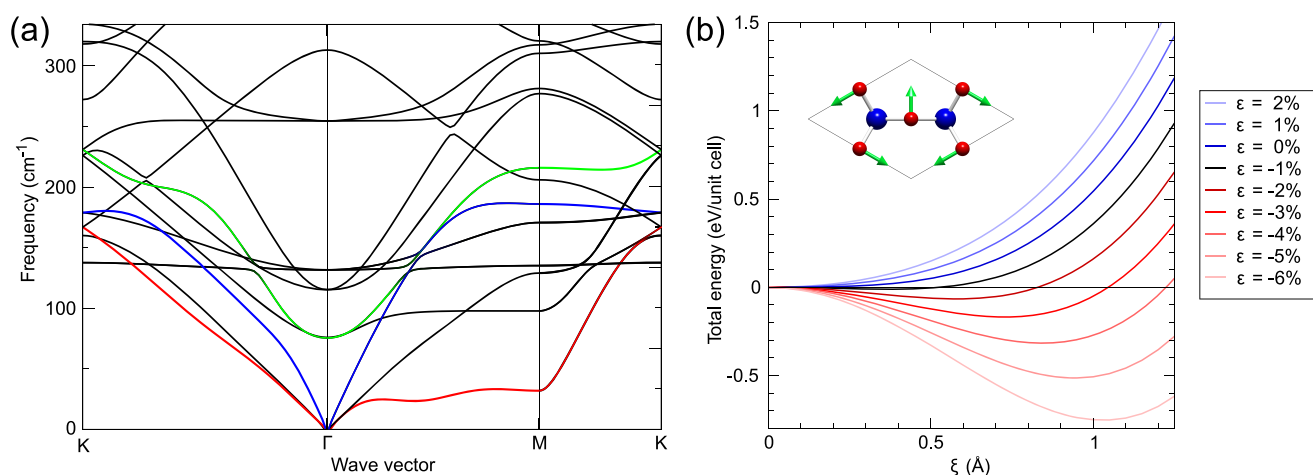


Figure 4. (a) Magnification of the low-energy part of the phonon dispersion graph in Figure 3(c), illustrating the kagome lattice modes described by Souslov *et al.*^{2,3} (b) Total energy as a function of the phonon normal mode coordinate, ξ , of the B_{2u} phonon mode for a series of biaxial strains. The figure shows only positive values of ξ , but the symmetry of the mode, shown as an inset, means that the curve is symmetric around zero. At zero temperature, the lattice immediately becomes unstable with respect to this displacement under compression, since the curve becomes a double well.

material being put on a substrate,¹⁷ or by disorder.¹⁸ We furthermore note that previous IR spectra reported by Löffler *et al.* for an “oxidized” sample⁵ similarly shows a small feature in the absorption near 1050 cm⁻¹, indicating that the most prominent Raman peak seen here may also be present in IR spectra.

To further investigate this symmetry breaking, we also performed calculations for two haeckelite structures, previously investigated in the context of the formation of the vitreous phase of 2D-SiO₂.¹⁹ These structures are formed by performing a Stone–Wales transformation in the smallest possible unit cell, to produce 2D crystal structures with a linkage different from the honeycomb lattice of the pristine system. Here, the haeckelite structures function as minimal prototypes of the disordered vitreous phase, or at least a phase where SiO₄ tetrahedra are connected at different angles. The analysis shows that the phonon DOS’s in the haeckelites are very similar to that of the pristine system (see Figure S4) and so do not provide direct help in ascertaining the degree of disorder from the Raman spectra. Inspection of the modes at the Γ point shows that the two IR modes retain the same character in the haeckelites as in the pristine system. The asymmetric bond-stretch mode at 1045 cm⁻¹ is found to correspond to a set of similar modes, which nevertheless somewhat hybridize with other modes (see Supporting Information Movie M1 and discussion in SI section IV). For other modes, such as the three-peak feature between 400 and 500 cm⁻¹, no clear correspondence to specific modes in the haeckelite structures is possible to identify by inspection. We conclude that the two IR modes are universal features of the bilayer silica structure irrespective of disorder of the ring arrangement, which is in agreement with previous analyses.⁵ The asymmetric bond-stretch mode is also to be expected in all cases, but some broadening of the peak should occur in the vitreous phase, as also seen in bulk structures.¹⁵ As for other modes identified in the pristine structure, a gradual broadening of the peaks should always be present upon going toward more disorder, but within the present analysis, we are not able to quantify the effect with sufficient precision to ascertain whether the three-peak structure at 400–500 cm⁻¹ is a uniquely defining feature of the pristine, hexagonal 2D-SiO₂ lattice or if it will also be

present in the vitreous phase. The possibility of using these peaks as a measure of disorder in the sample, in a manner similar to the *D* peak in graphene,²⁰ could be further investigated with access to samples with larger well-defined areas of pristine and vitreous phases of 2D-SiO₂.

The calculated phonon spectrum of pristine 2D-SiO₂ is shown in Figure 3c and is in fair agreement with the previous results of Zhou *et al.*²¹ The most important difference concerns the low-energy part of the spectrum, which in ref 21 contained an unstable mode, the lowest mode along the Γ -M path in Figure 3c. This is an important mode from the point of view of the stability of the lattice, since it is one of the modes that can be directly attributed to the dynamics of the kagome lattice. A magnified view of the low-energy phonon spectrum of Figure 3c is displayed in Figure 4a, related to rotations of the triangular building blocks of the kagome lattice, illustrated in Figure 1d. Souslov *et al.*² analyzed these modes, explaining that the kagome mode at highest energy at the Γ point (in green) comes from rigid rotations of the triangular units, the B_{2u} mode shown as inset in Figure 3a and in Figure S2b. Due to the bilayer structure of 2D-SiO₂, at the Γ point, this mode is degenerate with the B_{1g} mode in which the two kagome lattices rotate in opposite directions (Figure S2c). The B_{2u} mode hybridizes with one of the acoustic branches (red), so that the rotational motion of the B_{2u} is dominating the lowest-lying, red, branch at the *M* point.

It was previously noted that the 2D-SiO₂ lattice under compression “folds up”, with the oxygen tetrahedra rotating to accommodate the compressive strain,¹¹ thus forming a twisted kagome lattice as shown in Figure 1d. In the context of crystal vibrations, this can be expressed as the B_{1u} mode becoming unstable under compressive strain. Figure 4b explicitly shows the energy dependence on the B_{1u} normal mode coordinate, ξ , for a series of strains, and we can clearly see that the energy minimum is shifted away from zero, which corresponds to the nontwisted kagome lattice. We also note that the curve is very flat already at zero strain, hard to fit to a second degree polynomial, which indicates that anharmonic effects are important already in the ground state of the crystal. Anharmonicity leads to phonon–phonon interaction which at finite temperatures may serve to stabilize the crystal lattice.²²

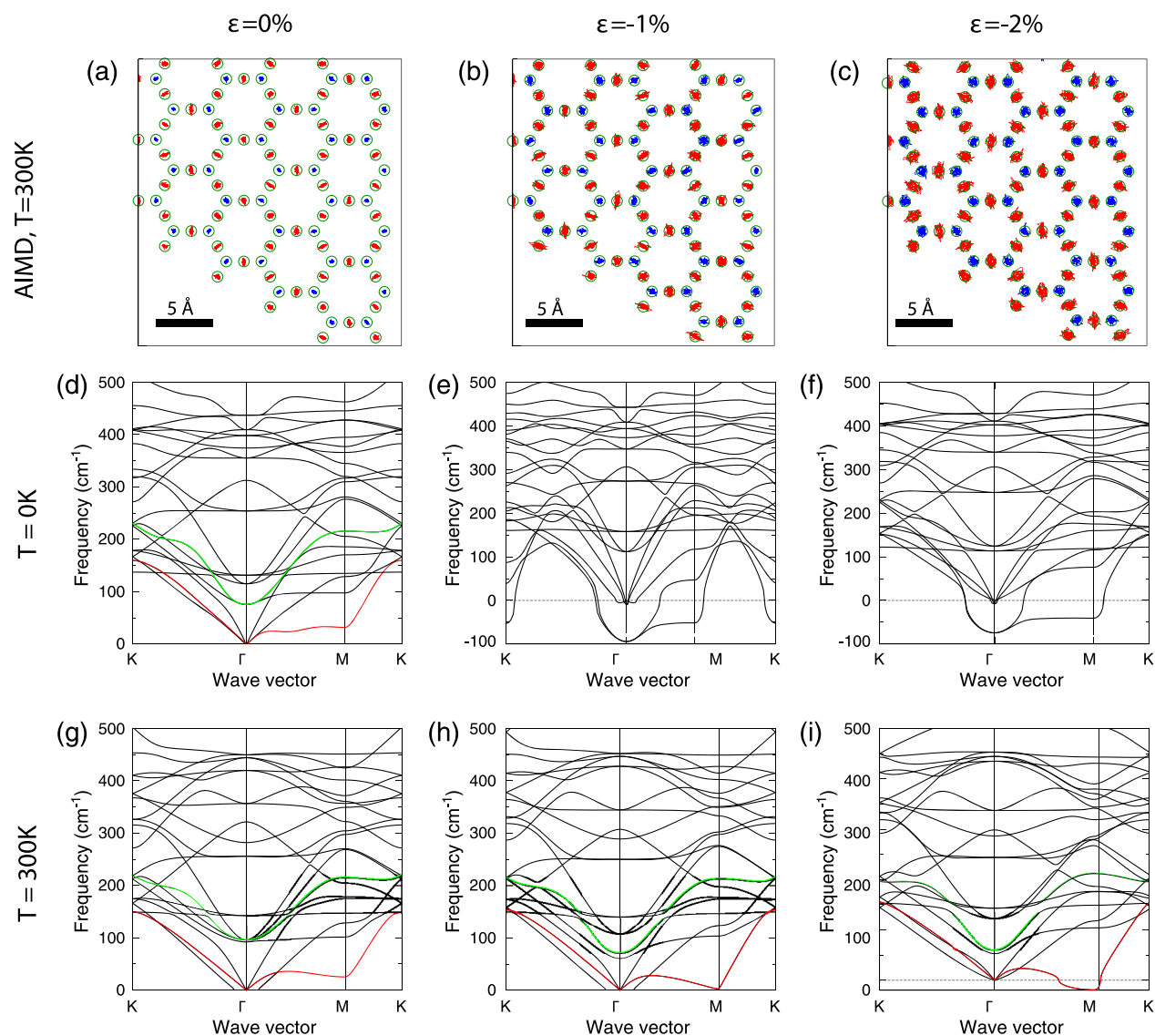


Figure 5. AIMD trajectories at a temperature of 300 K for compressive strains of 0%, 1%, and 2% (a–c), corresponding phonon spectra at temperatures of 0 K (d–f) and 300 K (g–i). The molecular dynamics trajectories show the structure in top view with Si atoms in blue, O atoms in red and green circles centered on the average atomic positions. The phonon spectra show the kagome modes in red and green immediately collapsing on compression at 0 K in (e) and (f). At room temperature, the kagome mode structure remains intact (g) and (h), with destabilization instead setting in at the *M* point at strains above about 2% (i).

To investigate finite temperature effects as a possible source of the discrepancy between calculated and experimental frequencies and also to gain further insights in the stability of the 2D-SiO₂ system, we performed *ab initio* molecular dynamics (AIMD) calculations at a temperature of 300 K for a series of biaxial strains. The AIMD trajectories obtained were then used to extract finite temperature effective force constant matrices with the TDEP method,^{23,24} to see finite-temperature effects on the vibrational spectrum.

Figure 5 illustrates the results of the AIMD calculations, showing particle trajectories and phonon spectra at $\epsilon = 0$ and for two compressive strains. From the AIMD trajectories, it is clear that the atoms spread out significantly around their average positions as the lattice is compressed, but that the average positions are those of the undistorted structure, with no apparent rotation of the tetrahedra. The oxygen atom trajectories form distributions which is not spherically symmetric around an average position, but rather ellipsoidal

in shape, spreading out in the direction perpendicular to the Si–O–Si bond. This corresponds to a significant occupation of phonon modes that rotate the oxygen tetrahedra. These rotational modes become stabilized by phonon–phonon interactions so that the free energy surface at room temperature remains a minimum at the B_{2u} normal mode coordinate $\xi = 0$ (inset of Figure 4b), in contrast to the 0 K result shown in Figures 4b and 5d.

This stability is explicitly demonstrated by effective phonon dispersion plots, shown in Figure 5d–i. At zero compressive strain ($\epsilon = 0$, Figure 5d,g), the spectra at 0 and 300 K are very similar, indicating that anharmonic effects are fairly small. At $\epsilon = -1\%$, Figure 5e shows that the kagome lattice collapses at 0 K. The two kagome modes that consist of rigid rotations of tetrahedra, shown in green and red, will merge into a single unstable mode at the Γ point. This results in the modes that extend to unphysical negative frequencies in Figure 5e,f, where the signature kagome modes are no longer present. By contrast,

Figure 5h clearly shows the kagome modes remaining clearly identifiable at 300 K, stabilized by phonon–phonon interactions at finite temperature. At $\epsilon = -2\%$ Figure S1 shows that the lattice does become unstable also at 300 K, but the distortion is not the simple rotation of the kagome lattice given by the B_{2u} mode at the Γ point, but through the lowest, flat kagome mode, shown in red in Figure 4a, and at the M point. This indicates that the distortion at finite temperature should involve a doubling of the unit cell along one of the axes and not be very large, a fact corroborated by the AIMD trajectories, which cannot show this small distortion on the time scale of the simulation. We also note that the softening of the phonon mode is much less drastic than is the case at 0 K, showing that the lattice is significantly stabilized at finite temperature. At sufficiently large compressive strain, about $\epsilon = -4\%$, the depth of the potential wells overcomes the thermal fluctuations. As a result, the kagome lattice folds up into a locked configuration (Figure S3), and the atoms become much more localized near their equilibrium positions.

Thus, the kagome lattice is stabilized at finite temperature by the inclusion of phonon–phonon interactions from the anharmonic potential induced by the compression. This stabilization mechanism is quite different from that earlier proposed for colloidal particles on a surface, based on a coarse-grained model that introduces the bending angle rigidity as a purely entropic term.²⁵ While such a picture may be valid for weakly interacting particles on a surface, where entropic contributions can be expected to dominate over direct interaction terms, it is clearly not applicable for the strongly bonded 2D-SiO₂. The introduction of a bending rigidity as a purely entropic contribution to the free energy makes it proportional to the temperature, which leads to an unstable lattice in the low-temperature limit, in clear contradiction with our 0 K results. Our results furthermore show that anharmonicity results in qualitative changes of the vibrational structure and is not a simple renormalization of the frequencies, as assumed by Mao *et al.*²⁵ A critical reexamination of the vibrational properties of the previously studied self-assembled polymer networks thus seems warranted.

At higher energies in the spectrum, the phonon DOS, including the optically active modes at the Γ point, is not significantly affected by temperature, so the underestimation of the calculated vibrational frequencies cannot be explained by anharmonic or other finite temperature effects. We suggest that the source may be that the lattice is stiffened by grain boundaries and other defects, which will locally lock and constrain the tetrahedra.¹⁹

CONCLUSIONS

In summary, using Raman spectroscopy and HR-TEM, we have identified several previously uncharacterized vibrational states of 2D-SiO₂, which have been assigned through comparison to DFT calculated spectra. These results enable Raman spectroscopy to be used as a quick and nondestructive method to identify the 2D-SiO₂ bilayer. The analysis indicates that these modes may be possible to use also to study the amount of disorder in the material, but further study is required for precise quantification of the effect. Our calculations also allow us to identify the phonon modes typical of a kagome lattice, and AIMD simulations reveal that the kagome lattice stability is strongly affected by phonon–phonon interactions at finite temperature. This provides fundamental insights into the

structural stability and properties of 2D-SiO₂ as well as kagome lattices in general.

METHODS AND MATERIALS

Computational Methods. Phonon spectra were calculated with the direct supercell method using the programs PHON²⁶ and PHONOPY,²⁷ with force constant matrices computed numerically with the Vienna *ab initio* simulation package^{28,29} and the projector-augmented wave method.^{30,31} Supercells of size $6 \times 6 \times 1$ were used in the force constant generation. A basis set cutoff of 800 eV for plane waves was used together with a k -space mesh of $12 \times 12 \times 1$ for Brillouin zone integration of the primitive cells, and on a $2 \times 2 \times 1$ mesh for the supercells, meaning that the supercell calculations were done on a k -point set equivalent to that used in the relaxation of the primitive cell. The electronic self-consistent field cycle was re-iterated until changes in energy were smaller than 10^{-8} eV, and the structure was relaxed until the maximal force on any atom was smaller than 0.001 eV/\AA^2 .

AIMD simulations were carried out in $5 \times 5 \times 1$ supercells using a k -point mesh only containing the Γ point and with a basis set cutoff of 300 eV. Calculations were done at 300 K by first equilibrating the system for about 1000 time steps in an NVE ensemble run and then continuing at fixed temperature with a Nosé–Hoover thermostat for approximately 10,000 time steps. Finite temperature phonon spectra were obtained from the molecular dynamics trajectories using the TDEP method of Hellman *et al.*^{23,24}

Sample Preparation. Graphene films were prepared with a low-pressure CVD technique using hexane as a precursor on polycrystalline Cu foils. The Cu foil was attached to a quartz substrate, which itself was placed into a quartz tube. The tube was pumped down to a pressure of 10–2 mbar. Then, forming gas (Ar/(5%)H₂) was introduced at a pressure of 5 mbar, and under these conditions, the Cu foil was heated up to 950 °C. When the desired temperature was achieved, the forming gas flow was interrupted, and hexane vapor was introduced into the quartz tube instead under a pressure of 0.5 mbar for 1 min. Finally, the sample was cooled down to room temperature under the flow of forming gas at a pressure of 5 mbar. The formation of a 2D layer of silica is attributed to an unintentional leakage of air into the quartz tube when switching from forming gas to hexane. This would cause the oxidation of the copper surface and a reaction with the quartz substrate at the contact surface with the oxidized copper. Albeit uncontrolled, these conditions seem sufficient to form the 2D layer of silica.

Transfer on TEM Grid. Graphene/silica films were transferred from the copper substrate by etching in 15% nitric acid and fishing the floating film (without polymer support) onto commercial TEM grids (Quantifoil R1.2/1.3 holey carbon film on Au 200 mesh). Afterward, the specimen was rinsed in distilled water dried in dry nitrogen. Prior to TEM, the samples were heated in air to 200 °C for 10 min.

Raman Spectroscopy. Raman measurements were performed with a scanning confocal setup where the laser beam of a solid state laser with a wavelength of 488 nm and a power of 7 mW was circularly polarized and focused to a diffraction-limited spot size of approximately 400 nm. While the position of the laser spot is fixed, the sample is raster scanned on a grid with a step size of 200 nm. At each position, the backscattered light is dispersed in a monochromator and detected with a Peltier cooled charge coupled device (CCD) with an accumulation time of 1 s.

Transmission Electron Microscopy. TEM experiments were performed with an image-side corrected FEI Titan 80–300 microscope operated at 80 kV. The spherical aberration was set to approximately 20 μm , and the energy spread of the source was reduced by lowering the extraction voltage to 2 kV. Dark-field imaging was a versatile tool to visualize details in the deposited layer at low and high magnifications.

ASSOCIATED CONTENT

S Supporting Information

The Supporting Information is available free of charge on the ACS Publications website at DOI: 10.1021/acsnano.6b05577.

Full Raman spectrum recorded, illustrations of phonon modes, illustrations of AIMD trajectories for a larger range of strains, all calculated phonon modes at the Γ -point, a comparison of phonon densities of states between the ordered 2D-SiO₂ phase and haeckelite structures (PDF)

Comparison of several modes of the ordered phase and haeckelite structures. (AVI)

AUTHOR INFORMATION

Corresponding Author

*E-mail: torbjorn.bjorkman@abo.fi.

ORCID 

Torbjörn Björkman: 0000-0002-1154-9846

Notes

The authors declare no competing financial interest.

ACKNOWLEDGMENTS

T.B. gratefully acknowledges Sergei Simak for providing the TDEP software. T.B. and A.V.K. acknowledge Academy of Finland funding through project 286279. V.S. acknowledges funding from the Austrian Science Fund (FWF) project AI0234411/21, and from the Slovak Scientific Grant Agency VEGA project 1/1004/15. J.M. acknowledges funding from the Austrian Science Fund (FWF) project P25721-N20. J.H.S. acknowledges support from the Graphene Flagship. Computational resources were provided by the Finland IT Centre for Science (CSC).

REFERENCES

- (1) Syözi, I. Statistics of Kagomé Lattice. *Prog. Theor. Phys.* **1951**, *6*, 306–308.
- (2) Souslov, A.; Liu, A. J.; Lubensky, T. C. Elasticity and Response in Nearly Isostatic Periodic Lattices. *Phys. Rev. Lett.* **2009**, *103*, 205503.
- (3) Sun, K.; Souslov, A.; Mao, X.; Lubensky, T. C. Surface Phonons, Elastic Response, and Conformal Invariance in Twisted Kagome Lattices. *Proc. Natl. Acad. Sci. U. S. A.* **2012**, *109*, 12369–12374.
- (4) Kane, C. L.; Lubensky, T. C. Topological Boundary Modes in Isostatic Lattices. *Nat. Phys.* **2014**, *10*, 39–45.
- (5) Löffler, D.; Uhlrich, J.; Baron, M.; Yang, B.; Yu, X.; Lichtenstein, L.; Heinke, L.; Büchner, C.; Heyde, M.; Shaikhutdinov, S.; Freund, H.-J.; Włodarczyk, R.; Sierka, M.; Sauer, J. Growth and Structure of Crystalline Silica Sheet on Ru(0001). *Phys. Rev. Lett.* **2010**, *105*, 146104.
- (6) Lichtenstein, L.; Büchner, C.; Yang, B.; Shaikhutdinov, S.; Heyde, M.; Sierka, M.; Włodarczyk, R.; Sauer, J.; Freund, H.-J. The Atomic Structure of a Metal-Supported Vitreous Thin Silica Film. *Angew. Chem., Int. Ed.* **2012**, *51*, 404–407.
- (7) Shaikhutdinov, S.; Freund, H.-J. Ultrathin Silica Films on Metals: The Long and Winding Road to Understanding the Atomic Structure. *Adv. Mater.* **2013**, *25*, 49–67.
- (8) Shaikhutdinov, S.; Freund, H.-J. Ultra-Thin Silicate Films on Metals. *J. Phys.: Condens. Matter* **2015**, *27*, 443001.
- (9) Freund, H.-J. The Surface Science of Catalysis and More, Using Ultrathin Oxide Films as Templates: A Perspective. *J. Am. Chem. Soc.* **2016**, *138*, 8985–8996.
- (10) Büchner, C.; Wang, Z.-J.; Burson, K. M.; Willinger, M.-G.; Heyde, M.; Schlögl, R.; Freund, H.-J. A Large-Area Transferable Wide Band Gap 2D Silicon Dioxide Layer. *ACS Nano* **2016**, *10*, 7982–7989.
- (11) Ben Romdhane, F.; Björkman, T.; Rodríguez-Manzo, J. A.; Cretu, O.; Krasheninnikov, A. V.; Banhart, F. In-Situ Growth of Cellular Two-Dimensional Silicon Oxide on Metal Substrates. *ACS Nano* **2013**, *7*, 5175–5180.
- (12) Huang, P. Y.; Kurasch, S.; Srivastava, A.; Skakalova, V.; Kotakoski, J.; Krasheninnikov, A. V.; Hovden, R.; Mao, Q.; Meyer, J. C.; Smet, J.; Müller, D. A.; Kaiser, U. Direct Imaging of a Two-Dimensional Silica Glass on Graphene. *Nano Lett.* **2012**, *12*, 1081–1086.
- (13) Lasaga, A. Optimization of CNDO for Molecular Orbital Calculation on Silicates. *Phys. Chem. Miner.* **1982**, *8*, 36–46.
- (14) Giordano, L.; Ricci, D.; Pacchioni, G.; Ugliengo, P. Structure and Vibrational Spectra of Crystalline SiO₂ Ultra-Thin Films on Mo(112). *Surf. Sci.* **2005**, *584*, 225–236.
- (15) Shcheblanov, N. S.; Mantis, B.; Umari, P.; Tanguy, A. Detailed Analysis of Plastic Shear in the Raman Spectra of SiO₂ Glass. *J. Non-Cryst. Solids* **2015**, *428*, 6–19.
- (16) He, R.; Wang, Z.; Qiu, R. L. J.; Delaney, C.; Beck, B.; Kidd, T. E.; Chancey, C. C.; Gao, X. P. A. Observation of Infrared-Active Modes in Raman Scattering from Topological Insulator Nanoplates. *Nanotechnology* **2012**, *23*, 455703.
- (17) Larentis, S.; Fallahzad, B.; Tutuc, E. Field-Effect Transistors and Intrinsic Mobility in Ultra-Thin MoSe₂ Layers. *Appl. Phys. Lett.* **2012**, *101*, 223104.
- (18) Skákalová, V.; Maultzsch, J.; Osváth, Z.; Biró, L. P.; Roth, S. Intermediate Frequency Modes in Raman Spectra of Ar+-Irradiated Single-Wall Carbon Nanotubes. *Phys. Status Solidi RRL* **2007**, *1*, 138–140.
- (19) Björkman, T.; Kurasch, S.; Lehtinen, O.; Kotakoski, J.; Yazyev, O. V.; Srivastava, A.; Skakalova, V.; Smet, J. H.; Kaiser, U.; Krasheninnikov, A. V. Defects in Bilayer Silica and Graphene: Common Trends in Diverse Hexagonal Two-Dimensional Systems. *Sci. Rep.* **2013**, *3*, 3482.
- (20) Ferrari, A. C.; Basko, D. M. Raman Spectroscopy as a Versatile Tool for Studying the Properties of Graphene. *Nat. Nanotechnol.* **2013**, *8*, 235–246.
- (21) Zhou, H.; Xi, Z.; Zhao, M. Theoretical Characterization of Layered Silica Nanostructures from First-Principles Prediction. *Phys. Lett. A* **2014**, *378*, 3348–3353.
- (22) Wallace, D. C. *Thermodynamics of Crystals*; Dover Publications: Mineola, NY, 1998.
- (23) Hellman, O.; Abrikosov, I. A.; Simak, S. I. Lattice Dynamics of Anharmonic Solids from First Principles. *Phys. Rev. B: Condens. Matter Mater. Phys.* **2011**, *84*, 180301.
- (24) Hellman, O.; Steneteg, P.; Abrikosov, I. A.; Simak, S. I. Temperature Dependent Effective Potential Method for Accurate Free Energy Calculations of Solids. *Phys. Rev. B: Condens. Matter Mater. Phys.* **2013**, *87*, 104111.
- (25) Mao, X.; Chen, Q.; Granick, S. Entropy Favours Open Colloidal Lattices. *Nat. Mater.* **2013**, *12*, 217–222.
- (26) Alfé, D. PHON: A Program to Calculate Phonons Using the Small Displacement Method. *Comput. Phys. Commun.* **2009**, *180*, 2622–2633.
- (27) Togo, A.; Oba, F.; Tanaka, I. First-Principles Calculations of the Ferroelastic Transition Between Rutile-Type and CaCl₂-Type SiO₂ at High Pressures. *Phys. Rev. B: Condens. Matter Mater. Phys.* **2008**, *78*, 134106.
- (28) Kresse, G.; Hafner, J. *Ab Initio* Molecular Dynamics for Liquid Metals. *Phys. Rev. B: Condens. Matter Mater. Phys.* **1993**, *47*, 558–561.
- (29) Kresse, G.; Furthmüller, J. Efficiency of *Ab-Initio* Total Energy Calculations for Metals and Semiconductors Using a Plane-Wave Basis Set. *Comput. Mater. Sci.* **1996**, *6*, 15–50.
- (30) Blöchl, P. E. Projector Augmented-Wave Method. *Phys. Rev. B: Condens. Matter Mater. Phys.* **1994**, *50*, 17953.
- (31) Kresse, G.; Joubert, D. From Ultrasoft Pseudopotentials to the Projector Augmented-Wave Method. *Phys. Rev. B: Condens. Matter Mater. Phys.* **1999**, *59*, 1758.